

# Unveiling Stripe-shaped Charge Modulations in Doped Mott Insulators

Ning Xia,<sup>1</sup> Yuchen Guo <sup>1</sup> and Shuo Yang <sup>1,2,3,\*</sup>

<sup>1</sup>State Key Laboratory of Low Dimensional Quantum Physics and Department of Physics, Tsinghua University, Beijing 100084, China

<sup>2</sup>Frontier Science Center for Quantum Information, Beijing 100084, China

<sup>3</sup>Hefei National Laboratory, Hefei 230088, China

Inspired by recent experimental findings, we investigate various scenarios of the doped Hubbard model with impurity potentials. We calculate the lattice Green's function in a finite-size cluster and then map it to the continuum real space, which allows for a direct comparison with scanning-tunneling-microscopy measurements on the local density of states. Our simulations successfully reproduce experimental data, including the characteristic stripe- and ladder-shaped structures observed in cuprate systems. Moreover, our results establish a connection between previous numerical findings on stripe-ordered ground states and experimental observations, thereby providing new insights into doped Mott insulators.

*Introduction.*— Understanding the high-temperature superconductivity in cuprates remains a fundamental challenge in condensed matter physics. Materials such as  $\text{YBa}_2\text{Cu}_3\text{O}_{6+y}$  (YBCO),  $\text{Bi}_2\text{Sr}_{2-x}\text{La}_x\text{CuO}_{6+y}$  (Bi2201), and  $\text{Ca}_{1-x}\text{Na}_x\text{CuO}_2\text{Cl}_2$  (NCCOC) exhibit a unified phase diagram. In the undoped region, they are Mott insulators with long-range antiferromagnetic order. Upon hole doping, they undergo a phase transition to become superconductors. This shared behavior suggests a common underlying mechanism within the cuprate family [1, 2].

Although phase fluctuation theory [1, 3] provides a framework for understanding the phase diagram of cuprates, the microscopic mechanisms driving the transition from Mott insulator to superconductor are not fully understood. A recent scanning tunneling microscopy (STM) experiment [4] on underdoped Bi2201 probes this critical region and observes modulations in local density of states (LDOS) near the Fermi energy. In the insulating sample with a hole concentration of  $p = 0.08$ , there is a spatial phase separation [5, 6] between the hole-free antiferromagnetic phase and the hole-rich phase. The spatial variations within the hole-rich region are highly analogous to those observed in the superconducting sample with  $p = 0.11$ . Specifically, the doped holes self-organize in short-range checkerboard order [7] with a wavelength of approximately  $4a_0$  (where  $a_0$  is the lattice constant of the  $\text{CuO}_2$  plane), and each plaquette in the checkerboard displays an internal stripe pattern [8, 9]. The primary difference between samples lies in the spatial occupation of the plaquettes. These findings suggest that plaquettes with internal stripe-shaped patterns are essential elementary building blocks. Moreover, even finer spatial structures including ladder- and clover-shaped patterns are observed at higher energy in lightly doped NCCOC [10], which are attributed to molecular orbitals embedded in a Mott insulator [11]. However, systematic investigations are necessary to corroborate their intuitive understanding.

From a theoretical perspective, the Hubbard model and  $t$ - $J$  model are considered minimal models that qualitatively capture the essence of cuprates [5, 6, 12–30]. At low doping levels, the ground state exhibits various charge orders [5, 23, 31],

including phase separation, uniform, and stripe configurations with energy close to each other and thus competitive. On the other hand, inhomogeneous impurity potentials of dopants can readily destroy the uniform state in realistic materials, thereby favoring phase separation. To further explain the spatial structures observed in experiments [4, 7, 10], previous studies investigate the ground state of these models in a finite-size cluster. For example, simulations using the density matrix renormalization group (DMRG) on the  $t$ - $J$  model [17] show that external potential fields can induce charge density modulations in the stripe state [20, 31–33], resembling the checkerboard state. With the Gutzwiller approximation, the Hubbard model also produces a checkerboard-like pattern [18]. However, differential conductance and LDOS measured with STM are related to the retarded Green's function in the continuum real space according to the linear response theory [34], which is not directly comparable to those numerically simulated ground state properties such as charge and spin distributions in a lattice system.

In this paper, inspired by experiments and the concept of molecular orbitals in Mott insulators [4, 10, 11], we investigate the stripe-ladder pattern of the doped Hubbard model with impurity potentials. We first employ the Chebyshev matrix product state (CheMPS) approach [35–37] to compute the retarded lattice Green's function. Subsequently, we apply a basis transformation [38, 39] to effectively map the Green's function to the continuum real space for direct comparison with experimental observations [10]. By tuning the impurity potentials in our simulations, we successfully reproduce the experimental data [10], particularly the newly discovered stripe-ladder pattern. This outcome offers new insights into the formation of stripe orders and demonstrates the potential of our approach to explain the complex behavior of cuprates.

*Model and method.*— We begin by interpreting the experimental data from Ref. [10]. As illustrated in Fig. 1(a, b), the underdoped sample with a hole concentration of  $p = 0.03$  exhibits phase separation into dark antiferromagnetic regions and bright hole-rich regions. In the hole-rich region of Fig. 1(a), two similar plaquettes emerge with an internal stripe-shaped pattern. In Fig. 1(b), a ladder-shaped pattern emerges in the same area. Moreover, a four-lobe clover-shaped pattern appears near the Na dopant marked by the magenta dot. In particular, this clover-shaped pattern is centered

\* shuoyang@tsinghua.edu.cn

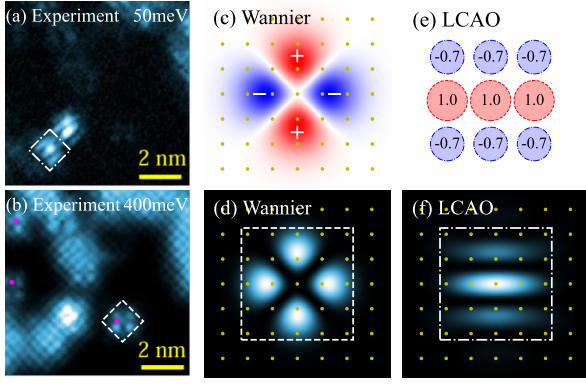


FIG. 1. (Color Online) (a-b) Experimental results of LDOS at 50meV (a) and 400meV (b), respectively, taken from Ref. [10]. (c-d) Density maps of the approximated Wannier function  $w_0(x,y)$  (c) and  $|w_0(x,y)|^2$  (d) at the surface exposed to the STM tip. Yellow dots represent Cu sites. (e) The coefficients for LCAO. (f) The density distribution of the LCAO wavefunction.

on the Cu sites, rather than the Na dopant [10].

Based on these observations, it is proposed that the clover-shaped pattern reflects the Wannier function of a single-hole state. For example, calculations in density functional theory (DFT) [38–40] show that the Wannier function exposed to the STM tip exhibits a consistent four-lobe-clover shape for different cuprate materials, regardless of the specific details near the  $\text{CuO}_2$  plane. To approximate this Wannier function, we use the symmetrized combination of  $p$ -orbital wave functions [41]. This choice is consistent with previous research on the sign of wave functions [38–40], and does not induce qualitative differences in our final results compared to the  $d$ -orbital wave functions. The density map of this approximated Wannier function  $w_0(x,y)$  is shown in Fig. 1(c) with  $d_{x^2-y^2}$  symmetry, whose density distribution  $|w_0(x,y)|^2$  is further illustrated in Fig. 1(d), displaying a four-lobe clover shape with its size adjusted to compare with experiments. Following the molecular orbital proposal in doped Mott insulators [10], we consider a linear combination of Wannier functions at different sites in analogy to the linear combination of atomic orbitals (LCAO) [42, 43], with coefficients shown in Fig. 1(e). The resulting molecular orbital has a stripe-shaped distribution (Fig. 1(f)) similar to that observed in experiments.

In short, the LCAO argument [42, 43] provides a preliminary understanding of the stripe-shaped pattern in experiments. The impurity potential introduced by the Na dopants creates a region that attracts holes, allowing the Wannier functions inside this region to play dominant roles in LCAO. However, systematic many-body numerical simulations instead of single-particle arguments are required to verify the emergence of stripe-shaped molecular orbitals. Therefore, we continue to consider the Hubbard model defined on a finite cluster

$$H = -t \sum_{\langle ij \rangle, \sigma} c_{i\sigma}^\dagger c_{j\sigma} - t' \sum_{\langle\langle ij \rangle\rangle, \sigma} c_{i\sigma}^\dagger c_{j\sigma} - \mu \sum_i n_i + U \sum_i (n_{i\uparrow} - \frac{1}{2})(n_{i\downarrow} - \frac{1}{2}) + \sum_i V_i n_i, \quad (1)$$

where we set typical parameters  $t = 1.0$ ,  $t' = -0.3$ , and  $U = 12$  [18, 21, 44, 45]. The number of holes is controlled using  $U(1)$  symmetry [46, 47]. The chemical potential  $\mu$  is tuned to ensure the ground state with the desired hole number being the true ground state of the entire system [19, 48–50]. Local potential fields  $V_i$  are applied to certain lattice sites to simulate impurity effects.

To solve this model and reproduce the experimental data, we first implement the standard DMRG procedure to obtain the ground state  $|\Omega\rangle$  with energy  $E_0$  and hole number  $N_0$ . We then apply the CheMPS method [35–37, 51] to compute the retarded lattice Green's function  $G_{ij,\sigma}^R(\omega) = G_{ij,\sigma}^+(\omega) - G_{ij,\sigma}^-(\omega)$ . Here,

$$G_{ij,\sigma}^+(\omega) = \langle \Omega | c_{i\sigma} \frac{1}{(\omega + i0^+) + (E_0 - H)} c_{j\sigma}^\dagger | \Omega \rangle, \quad (2)$$

$$G_{ij,\sigma}^-(\omega) = \langle \Omega | c_{j\sigma}^\dagger \frac{1}{-(\omega + i0^+) + (E_0 - H)} c_{i\sigma} | \Omega \rangle.$$

After that, we convert the retarded lattice Green's function to a continuum real-space representation by [38, 39]

$$G_\sigma^R(\mathbf{r}, \mathbf{r}', \omega) = \sum_{ij} w_i(\mathbf{r}) w_j^*(\mathbf{r}') G_{ij,\sigma}^R(\omega), \quad (3)$$

where  $w_i(\mathbf{r})$  is the Wannier function centered at the  $i$ -th Cu site. The LDOS  $\rho(\mathbf{r}, E) = -\sum_\sigma \text{Im} G_\sigma^R(\mathbf{r}, \mathbf{r}, E) / \pi$  is proportional to the STM differential conductance  $dI/dV$ , allowing for direct comparisons.

Although the results presented in this manuscript are calculated using a finite cluster with open boundary conditions, we also use a hybrid approach [52] combining CheMPS [35–37] and cluster perturbation theory (CPT) [53–55] to study larger systems. The main conclusions remain qualitatively unchanged, suggesting that the physical phenomena observed in the finite cluster are robust and not artifacts of the finite-size simulation.

*Numerical results.*— We perform simulations of doped holes in finite clusters, including three scenarios based on the number of doped holes: the one-hole, two-hole and four-hole cases. In the one-hole case, we first apply a strong potential field to a single lattice site to pin the doped hole for a  $4 \times 4$  cluster as shown in Fig. 2(a), whose results are illustrated in Fig. 2(b-d). The density of states (DOS) is shown in Fig. 2(b), where the lower Hubbard band lies below energy 0 and the upper Hubbard band lies above energy  $7t_0$ . Doping-induced in-gap states appear between these two bands, with two distinct peaks marked by red and blue arrows. The real space structures of these peaks are visualized in Fig. 2(c) and Fig. 2(d), respectively. The LDOS for the lower energy peak exhibits a four-lobe clover pattern identical to the shape of the Wannier function, centered at the Cu site where the potential field is applied (Fig. 2(c)). This result indicates that a sufficiently localized hole indeed manifests the shape of the Wannier function, consistent with the experimental results in Fig. 2(e). In contrast, the LDOS for the higher energy peak shows a halved clover pattern in Fig. 2(d), reflecting the transfer of spectral weight from the upper Hubbard band upon doping [56, 57]. These features are qualitatively comparable with

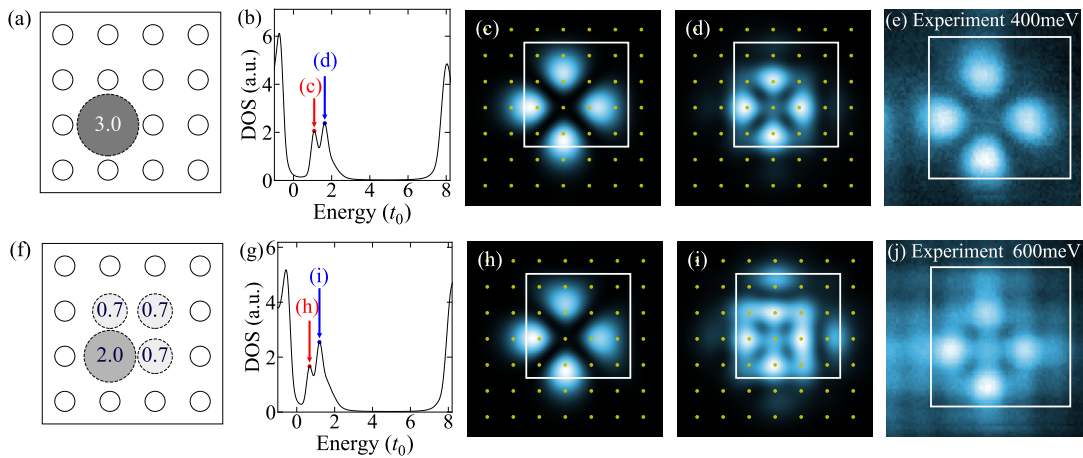


FIG. 2. (Color Online) (a-d) The first one-hole case with chemical potential  $\mu = -3.7t_0$ . (a) Model defined on a  $4 \times 4$  cluster, with circles representing Cu sites. Local potential fields  $V_i$  are applied in gray circles, with radii proportional to  $|V_i|$ . (b) DOS for the first one-hole case. (c-d) The LDOS at two peaks in (b). The sites inside the white box correspond to those calculated during the simulation. (f-i) Results for the second one-hole case with chemical potential  $\mu = -3.7t_0$ . (e, j) Experimental LDOS for lower energy at 400meV (e) and for higher energy at 600meV (j), taken from Ref. [10].

Fig. 2(j), while the doped hole spreads more extensively at higher energy in the experimental results, particularly within and outside the clover-shaped pattern.

To better simulate the higher-energy structure, we consider an additional set of parameters in Fig. 2(f). Ideally, the potential field generated by the Na dopant is symmetric with respect to the nearest-neighbor Cu sites [58, 59] (Fig. S1(a) in Supplemental Material [51]), while experiments [10] suggest that the nearby dopants and defects can break this symmetry. Taking this into account, we apply potential fields  $V_i$  to four nearby lattice sites, with one dominant over others. The DOS of the in-gap state in Fig. 2(g) still shows two characteristic peaks. For the lower energy peak shown in Fig. 2(h), it exhibits a clover-shaped distribution centered at the Cu site, where the potential field is strongest. For the higher energy peak in Fig. 2(i), four sites with higher hole density display a halved clover shape similar to that in Fig. 2(d). However, the density distribution here is more extensive and thus better reproduces the experimental results in Fig. 2(j), suggesting that the effective impurity potentials in experiments may have a distribution similar to that in Fig. 2(f).

Moving on to the two-hole case, we aim to verify that the observed stripe-shaped pattern reflects the molecular orbital embedded in the Mott insulator. We consider a  $5 \times 4$  cluster shown in Fig. 3(a), with impurity potential fields  $V_i$  applied to the inner  $3 \times 2$  region and dominant on one side, mimicking the effects of other impurities. The DOS in Fig. 3(b) shows a gap structure near the Fermi energy, with the part below 0 related to the lower Hubbard band and the part above 0 associated with the in-gap state. The peak at energy  $0.32t_0$  as a characteristic lower-energy state and a higher-energy state at  $0.8t_0$  for reference are marked by red and blue arrows. The lower-energy LDOS in Fig. 3(c) shows a three-stripe pattern, resembling an alternative LCAO outcome depicted in Fig. 3(e, f), where the Wannier functions form an in-phase superposition analogous to that of a bonding molec-

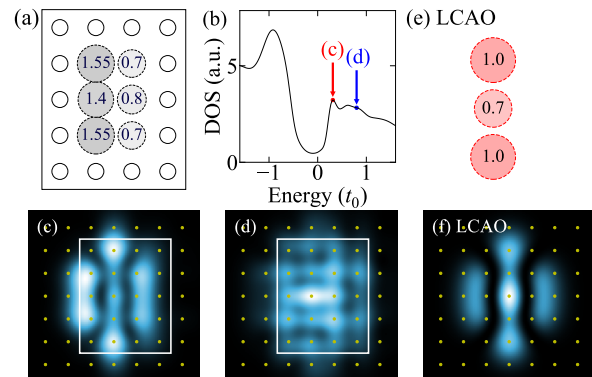


FIG. 3. (Color Online) Two-hole case with chemical potential  $\mu = -3.7t_0$ . (a) Model defined on a  $5 \times 4$  cluster. (b) DOS of the two-hole case. (c-d) LDOS at energies highlighted by the red and blue arrows in (b). (e) LCAO coefficients. (f) Density distribution of the LCAO result.

ular orbital. For the higher-energy state in Fig. 3(d), we see a ladder-shaped distribution of LDOS perpendicular to the lower-energy stripe-shaped distribution, which corresponds to an antibonding molecular orbital and agrees with the experimental results.

We successfully reproduce the stripe-ladder pattern in the two-hole case (more results in Fig. S2 [51]). However, to demonstrate the checkerboard structure with an internal stripe-ladder pattern, we need to consider a minimal four-hole case. In this scenario, a larger number of dopants will induce smoother local potential fields. To simulate this, we trap four holes inside a  $10 \times 4$  cluster with broad potential fields, as shown in Fig. 4(a). We first calculate the hole densities  $1 - \langle n_{i\uparrow} + n_{i\downarrow} \rangle$  and the magnetic moments  $\frac{1}{2} \langle n_{i\uparrow} - n_{i\downarrow} \rangle$  for our ground state in Fig. 4(b). The hole density is concentrated mainly in the central  $8 \times 2$  region with slight modulations, and

this region also forms a domain wall of the surrounding antiferromagnetism [60]. It indicates that the ground state is indeed a stripe state, consistent with previous numerical results for the  $t$ - $J$  model [17].

In addition, the stripe state is deemed relevant to the checkerboard structure observed in experiments [17]. By simulating spectral functions, we better demonstrate this correspondence through the characteristic features of excited states that exhibit checkerboard plaquettes with internal stripe-ladder patterns. In particular, Fig. 4(c) shows the DOS around the Fermi energy, which displays a U-shaped gap structure. Due to the large degrees of freedom in this system, characteristic peaks are no longer clearly visible. Therefore, we highlight two typical energies at  $0.45t_0$  and  $0.9t_0$ , marked with red and blue arrows. We plot the LDOS for these two energies in Fig. 4(d) and Fig. 4(e), respectively. At lower energy, we find that the DOS exhibits two plaquettes with three stripes inside each plaquette. This pattern qualitatively replicates the experimental data shown in Fig. 4(f). Notably, the lengths and intensities of these three stripes are roughly equivalent. This result is in contrast to the two-hole case depicted in Fig. 3(c), where the central stripe is longer and less intense. The similarity between our simulated data and the experimental results suggests that in the four-hole case, the pairs of holes in two plaquettes interact with each other, resulting in a shorter and thicker central stripe. This result highlights the role played by the interaction between holes in forming such a many-body pattern. At higher energy, we observe an LDOS pattern that exhibits a ladder-shaped distribution, as shown in Fig. 4(e). This qualitative agreement with the experimental data (Fig. 4(g)) indicates that our simulations capture the essence of experimental phenomena (more results in Fig. S3 [51]). These findings demonstrate the ability of our simulations to model and predict the behavior of this complex system, providing valuable insights into the underlying physics.

*Conclusion and discussion.*— In summary, we employ the CheMPS method to simulate the retarded lattice Green’s functions for various hole-doping cases in the doped Hubbard model with impurity potential fields. Our calculations enable the projection of the LDOS onto the continuum real space, allowing for a direct and accurate comparison with the STM experiments. We find that the single-hole state exhibits a four-lobe clover pattern in its lowest in-gap state. In contrast, the two-hole state forms a stripe-ladder pattern, which is strikingly similar to the bonding and antibonding molecular orbitals formed by the dimerization of two holes. This result is consistent with experimental observations. Notably, the four-hole state shows two distinct LDOS patterns depending on the energy range. At lower energy, we observe two stripe-shaped plaquettes that are characteristic of the interaction and correlation between the pair of holes. At higher energy, a ladder-shaped structure emerges, in agreement with previous experimental studies [10]. Our calculations also reveal the hole densities and magnetic moments of the ground state, which exhibit a slightly modulated stripe order. This result is consistent with previous numerical calculations using the  $t$ - $J$  model [17], further confirming the validity of our simulations.

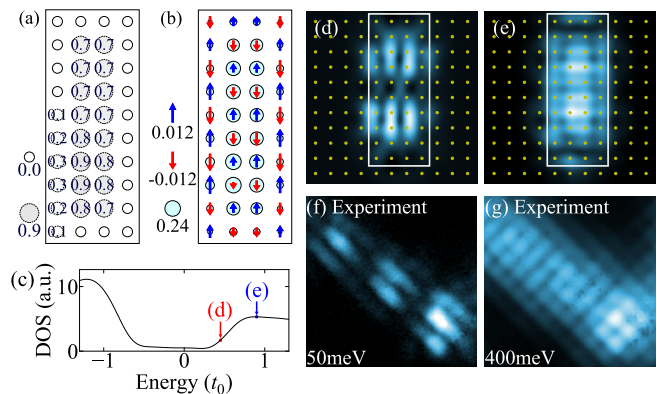


FIG. 4. (Color Online) Four-hole case with chemical potential  $\mu = -3.7t_0$ . (a) Model defined on a  $10 \times 4$  cluster. (b) The hole densities and the magnetic moments of the ground state. The circle and arrows outside the box illustrate the maximums of the hole densities and the magnetic moments, respectively. (c) DOS of the four-hole case. (d-e) LDOS at energies indicated by the arrows in (c). (f-g) Experimental LDOS for lower energy at 50meV (f) and for higher energy at 400meV (g), taken from Ref. [10].

As proposed in Ref. [10, 11], the stripe-ladder patterns of the doped holes exhibit striking similarities to molecular orbitals embedded in antiferromagnetic Mott insulators. Our simulations not only provide supportive evidence for this proposal, but also offer a unique perspective on the many-body physics involved. Specifically, our results imply that doped holes occupying such molecular orbitals can give rise to a many-body ground state with stripe order [17, 60]. A particularly intriguing feature of our finding is the presence of a stripe-shaped plaquette containing two holes, suggesting a possible pairing structure in the ground state. This result resonates with recent theoretical studies that propose paired twisted holes as a mechanism for charge order in doped Mott insulators [24, 26–28]. To gain a deeper understanding of this phenomenon, more research is needed to explore the properties of excitations in doped Mott insulators.

Our study successfully bridges the gap between numerical simulations and experimental observations, providing new insights into the intricate interplay between antiferromagnetism and charge order. We believe that our results will provide inspiration for future related research and shed light on the complex physics of strongly correlated systems, ultimately contributing to a better understanding of doped Mott insulators.

*Note added.*— As we finalize this manuscript, we become aware of an independent study focusing on the three-band Hubbard model [61]. Their investigation reveals that the in-gap state exhibits a four-lobe clover-shaped pattern in LDOS, which they attribute to the localized Zhang-Rice singlet. This finding is consistent with our choice of basis for the one-band Hubbard model and our interpretation for a localized single hole.

## ACKNOWLEDGMENTS

*Acknowledgement.*— We thank Shusen Ye and Yayu Wang for helpful discussions and providing STM data. We also

thank Zheng-Yu Weng for useful suggestions. This work is supported by the National Natural Science Foundation of China (NSFC) (Grant No. 12174214 and No. 92065205) and the Innovation Program for Quantum Science and Technology (Grant No. 2021ZD0302100).

- 
- [1] P. A. Lee, N. Nagaosa, and X.-G. Wen, Doping a Mott insulator: Physics of high-temperature superconductivity, *Rev. Mod. Phys.* **78**, 17 (2006).
- [2] C. Proust and L. Taillefer, The remarkable underlying ground states of cuprate superconductors, *Annu. Rev. Condens. Matter Phys.* **10**, 409 (2019).
- [3] V. Emery and S. Kivelson, Importance of phase fluctuations in superconductors with small superfluid density, *Nature* **374**, 434 (1995).
- [4] S. Ye, C. Zou, H. Yan, Y. Ji, M. Xu, Z. Dong, Y. Chen, X. Zhou, and Y. Wang, The emergence of global phase coherence from local pairing in underdoped cuprates, *Nat. Phys.* **19**, 1301 (2023).
- [5] V. J. Emery, S. A. Kivelson, and H. Q. Lin, Phase separation in the  $t$ - $J$  model, *Phys. Rev. Lett.* **64**, 475 (1990).
- [6] E. Dagotto, Correlated electrons in high-temperature superconductors, *Rev. Mod. Phys.* **66**, 763 (1994).
- [7] T. Hanaguri, C. Lupien, Y. Kohsaka, D.-H. Lee, M. Azuma, M. Takano, H. Takagi, and J. C. Davis, A ‘checkerboard’ electronic crystal state in lightly hole-doped  $\text{Ca}_{2-x}\text{Na}_x\text{CuO}_2\text{Cl}_2$ , *Nature* **430**, 1001 (2004).
- [8] H. Li, H. Li, Z. Wang, S. Wan, H. Yang, and H.-H. Wen, Low-energy gap emerging from confined nematic states in extremely underdoped cuprate superconductors, *npj Quantum Mater.* **8**, 18 (2023).
- [9] J. Zaanen, High  $T_c$  superconductivity in Copper oxides: the condensing bosons as stripy plaquettes, *npj Quantum Mater.* **8**, 26 (2023).
- [10] S. Ye, J. Zhao, Z. Yao, S. Chen, Z. Dong, X. Li, L. Shi, Q. Liu, C. Jin, and Y. Wang, Visualizing the Zhang-Rice singlet, molecular orbitals and pair formation in cuprate (2023), [arXiv:2309.09260](https://arxiv.org/abs/2309.09260).
- [11] H. Li, S. Ye, J. Zhao, C. Jin, and Y. Wang, Imaging the atomic-scale electronic states induced by a pair of hole dopants in  $\text{Ca}_2\text{CuO}_2\text{Cl}_2$  Mott insulator, *Sci. Bull.* **66**, 1395 (2021).
- [12] D. P. Arovas, E. Berg, S. A. Kivelson, and S. Raghu, The Hubbard Model, *Annu. Rev. Condens. Matter Phys.* **13**, 239 (2022).
- [13] H.-D. Chen, S. Capponi, F. Alet, and S.-C. Zhang, Global phase diagram of the high- $T_c$  cuprates, *Phys. Rev. B* **70**, 024516 (2004).
- [14] H.-D. Chen, J.-P. Hu, S. Capponi, E. Arrighoni, and S.-C. Zhang, Antiferromagnetism and Hole Pair Checkerboard in the Vortex State of High  $T_c$  Superconductors, *Phys. Rev. Lett.* **89**, 137004 (2002).
- [15] H.-D. Chen, O. Vafek, A. Yazdani, and S.-C. Zhang, Pair Density Wave in the Pseudogap State of High Temperature Superconductors, *Phys. Rev. Lett.* **93**, 187002 (2004).
- [16] P. W. Anderson, A suggested 4 x 4 structure in underdoped cuprate superconductors: a wigner supersolid (2004), [arXiv:cond-mat/0406038](https://arxiv.org/abs/cond-mat/0406038).
- [17] S. R. White and D. J. Scalapino, Checkerboard patterns in the  $t$ - $J$  model, *Phys. Rev. B* **70**, 220506 (2004).
- [18] G. Seibold, J. Lorenzana, and M. Grilli, Checkerboard and stripe inhomogeneities in cuprates, *Phys. Rev. B* **75**, 100505 (2007).
- [19] M. Qin, C.-M. Chung, H. Shi, E. Vitali, C. Hubig, U. Schollwöck, S. R. White, and S. Zhang (Simons Collaboration on the Many-Electron Problem), Absence of Superconductivity in the Pure Two-Dimensional Hubbard Model, *Phys. Rev. X* **10**, 031016 (2020).
- [20] Z.-T. Xu, Z.-C. Gu, and S. Yang, Competing orders in the honeycomb lattice  $t$ - $J$  model, *Phys. Rev. B* **108**, 035144 (2023).
- [21] M. Qin, T. Schäfer, S. Andergassen, P. Corboz, and E. Gull, The Hubbard Model: A Computational Perspective, *Annu. Rev. Condens. Matter Phys.* **13**, 275 (2022).
- [22] H. Xu, C.-M. Chung, M. Qin, U. Schollwöck, S. R. White, and S. Zhang, Coexistence of superconductivity with partially filled stripes in the Hubbard model, *Science* **384**, eadh7691 (2024).
- [23] S. R. White and D. J. Scalapino, Phase separation and stripe formation in the two-dimensional  $t$ - $J$  model: A comparison of numerical results, *Phys. Rev. B* **61**, 6320 (2000).
- [24] J.-Y. Zhao, S. A. Chen, H.-K. Zhang, and Z.-Y. Weng, Two-Hole Ground State: Dichotomy in Pairing Symmetry, *Phys. Rev. X* **12**, 011062 (2022).
- [25] X. Lu, F. Chen, W. Zhu, D. N. Sheng, and S.-S. Gong, Emergent Superconductivity and Competing Charge Orders in Hole-Doped Square-Lattice  $t$ - $J$  Model, *Phys. Rev. Lett.* **132**, 066002 (2024).
- [26] J.-Y. Zhao and Z.-Y. Weng, Distinct quasiparticle excitations in single-particle spectral function (2023), [arXiv:2309.11556](https://arxiv.org/abs/2309.11556).
- [27] D. N. Sheng, Y. C. Chen, and Z. Y. Weng, Phase String Effect in a Doped Antiferromagnet, *Phys. Rev. Lett.* **77**, 5102 (1996).
- [28] Z. Y. Weng, D. N. Sheng, Y.-C. Chen, and C. S. Ting, Phase string effect in the  $t$ - $J$  model: General theory, *Phys. Rev. B* **55**, 3894 (1997).
- [29] Z.-T. Xu, Z.-C. Gu, and S. Yang, Global phase diagram of doped quantum spin liquid on the Kagome lattice (2024), [arXiv:2404.05685](https://arxiv.org/abs/2404.05685).
- [30] Z.-Y. Yue, Z.-T. Xu, S. Yang, and Z.-C. Gu, Pseudogap phase as fluctuating pair density wave (2024), [arXiv:2404.16770](https://arxiv.org/abs/2404.16770).
- [31] B.-X. Zheng, C.-M. Chung, P. Corboz, G. Ehlers, M.-P. Qin, R. M. Noack, H. Shi, S. R. White, S. Zhang, and G. K.-L. Chan, Stripe order in the underdoped region of the two-dimensional Hubbard model, *Science* **358**, 1155 (2017).
- [32] P. Corboz, T. M. Rice, and M. Troyer, Competing States in the  $t$ - $J$  model: Uniform  $d$ -wave State versus Stripe State, *Phys. Rev. Lett.* **113**, 046402 (2014).
- [33] S. R. White and D. J. Scalapino, Ground states of the doped four-leg  $t$ - $J$  ladder, *Phys. Rev. B* **55**, R14701 (1997).
- [34] O. Fischer, M. Kugler, I. Maggio-Aprile, C. Berthod, and C. Renner, Scanning tunneling spectroscopy of high-temperature superconductors, *Rev. Mod. Phys.* **79**, 353 (2007).
- [35] A. Holzner, A. Weichselbaum, I. P. McCulloch, U. Schollwöck, and J. von Delft, Chebyshev matrix product state approach for spectral functions, *Phys. Rev. B* **83**, 195115 (2011).
- [36] A. Braun and P. Schmitteckert, Numerical evaluation of Green’s functions based on the Chebyshev expansion, *Phys. Rev. B* **90**, 165112 (2014).

- [37] P.-Y. Zhao, K. Ding, and S. Yang, Chebyshev pseudosite matrix product state approach for the spectral functions of electron-phonon coupling systems, *Phys. Rev. Res.* **5**, 023026 (2023).
- [38] P. Choubey, T. Berlijn, A. Kreisel, C. Cao, and P. J. Hirschfeld, Visualization of atomic-scale phenomena in superconductors: Application to FeSe, *Phys. Rev. B* **90**, 134520 (2014).
- [39] A. Kreisel, P. Choubey, T. Berlijn, W. Ku, B. M. Andersen, and P. J. Hirschfeld, Interpretation of Scanning Tunneling Quasiparticle Interference and Impurity States in Cuprates, *Phys. Rev. Lett.* **114**, 217002 (2015).
- [40] P. Choubey, A. Kreisel, T. Berlijn, B. M. Andersen, and P. J. Hirschfeld, Universality of scanning tunneling microscopy in cuprate superconductors, *Phys. Rev. B* **96**, 174523 (2017).
- [41] F. C. Zhang and T. M. Rice, Effective Hamiltonian for the superconducting Cu oxides, *Phys. Rev. B* **37**, 3759 (1988).
- [42] R. Hoffmann, *Solids and surfaces: a chemist's view of bonding in extended structures* (John Wiley & Sons, 2021).
- [43] R. Hoffmann, A chemical and theoretical way to look at bonding on surfaces, *Rev. Mod. Phys.* **60**, 601 (1988).
- [44] W.-G. Yin and W. Ku, Tuning the in-plane electron behavior in high- $T_c$  cuprate superconductors via apical atoms: A first-principles Wannier-states analysis, *Phys. Rev. B* **79**, 214512 (2009).
- [45] K. Tanaka, T. Yoshida, A. Fujimori, D. H. Lu, Z.-X. Shen, X.-J. Zhou, H. Eisaki, Z. Hussain, S. Uchida, Y. Aiura, K. Ono, T. Sugaya, T. Mizuno, and I. Terasaki, Effects of next-nearest-neighbor hopping  $t'$  on the electronic structure of cuprate superconductors, *Phys. Rev. B* **70**, 092503 (2004).
- [46] S. Singh, R. N. C. Pfeifer, and G. Vidal, Tensor network states and algorithms in the presence of a global U(1) symmetry, *Phys. Rev. B* **83**, 115125 (2011).
- [47] M. Fishman, S. R. White, and E. M. Stoudenmire, The ITensor Software Library for Tensor Network Calculations, *SciPost Phys. Codebases* , 4 (2022).
- [48] S. Chiesa, P. B. Chakraborty, W. E. Pickett, and R. T. Scalettar, Disorder-Induced Stabilization of the Pseudogap in Strongly Correlated Systems, *Phys. Rev. Lett.* **101**, 086401 (2008).
- [49] M. N. Gastiasoro and B. M. Andersen, Enhancing superconductivity by disorder, *Phys. Rev. B* **98**, 184510 (2018).
- [50] J. C. Szabo, K. Lee, V. Madhavan, and N. Trivedi, Local Spectroscopies Reveal Percolative Metal in Disordered Mott Insulators, *Phys. Rev. Lett.* **124**, 137402 (2020).
- [51] See supplemental material for details.
- [52] P.-Y. Zhao, K. Ding, and S. Yang, Chebyshev pseudosite matrix product state approach for cluster perturbation theory (2024), [arXiv:2404.05686](https://arxiv.org/abs/2404.05686).
- [53] W.-H. Leong, S.-L. Yu, T. Xiang, and J.-X. Li, Localized in-gap state in a single-electron doped Mott insulator, *Phys. Rev. B* **90**, 245102 (2014).
- [54] D. Sénéchal, D. Perez, and D. Plouffe, Cluster perturbation theory for Hubbard models, *Phys. Rev. B* **66**, 075129 (2002).
- [55] D. Sénéchal, D. Perez, and M. Pioro-Ladrière, Spectral Weight of the Hubbard Model through Cluster Perturbation Theory, *Phys. Rev. Lett.* **84**, 522 (2000).
- [56] P. W. Anderson, "Luttinger-liquid" behavior of the normal metallic state of the 2D Hubbard model, *Phys. Rev. Lett.* **64**, 1839 (1990).
- [57] M. B. J. Meinders, H. Eskes, and G. A. Sawatzky, Spectral-weight transfer: Breakdown of low-energy-scale sum rules in correlated systems, *Phys. Rev. B* **48**, 3916 (1993).
- [58] K. J. von Szczepanski, T. M. Rice, and F. C. Zhang, Impurity States in the  $(t, J)$ -Model, *Europhys. Lett.* **8**, 797 (1989).
- [59] Y. Chen, T. M. Rice, and F. C. Zhang, Rotational Symmetry Breaking in the Ground State of Sodium-Doped Cuprate Superconductors, *Phys. Rev. Lett.* **97**, 237004 (2006).
- [60] J. Zaanen and O. Gunnarsson, Charged magnetic domain lines and the magnetism of high- $T_c$  oxides, *Phys. Rev. B* **40**, 7391 (1989).
- [61] P. Li, Y. Shen, M. Qin, K. Jiang, J. Hu, and T. Xiang, Bound states in doped charge transfer insulators (2024), [arXiv:2408.00576](https://arxiv.org/abs/2408.00576).
- [62] A. Weiße, G. Wellein, A. Alvermann, and H. Fehske, The kernel polynomial method, *Rev. Mod. Phys.* **78**, 275 (2006).
- [63] U. Schollwöck, The density-matrix renormalization group in the age of matrix product states, *Ann. Phys.* **326**, 96 (2011).

## Supplemental Material

This Supplemental Material offers an in-depth explanation of the CheMPS method in Appendix A. Furthermore, we conduct a thorough analysis of LDOS distributions under various conditions. Appendices B-D showcase how the real-space patterns in LDOS evolve with these parameters.

### Appendix A: Chebyshev Matrix Product State Method

The quantity we aim to calculate is the lattice Green's function  $G_{ij,\sigma}(z) = G_{ij,\sigma}^+(z) - G_{ij,\sigma}^-(z)$ .

$$\begin{aligned} G_{ij,\sigma}^+ &= \langle \psi_0 | c_{i\sigma} \frac{1}{z + (E_0 - H)} c_{j\sigma}^\dagger | \psi_0 \rangle, \\ G_{ij,\sigma}^- &= \langle \psi_0 | c_{j\sigma}^\dagger \frac{1}{-z + (E_0 - H)} c_{i\sigma} | \psi_0 \rangle. \end{aligned} \quad (S1)$$

Here,  $|\psi_0\rangle$  is the ground state with energy  $E_0$ . The retarded Green's function can be obtained by setting  $z = \omega + i\eta$  in  $G_{ij,\sigma}(z)$ . We implement the CheMPS method [35–37] to calculate the lattice Green's function. In the following, we illustrate how to compute  $G_{ij,\sigma}^+(z)$ . First, we choose an appropriate energy window  $[-\omega_1, \omega_2]$  and perform a rescaling transformation for the variable  $z$  and the Hamiltonian  $H$ .

$$\begin{aligned} z \mapsto z' &= \omega' + i\eta/a, \quad \omega' = \frac{\omega}{a} + b, \\ H \mapsto H' &= \frac{H - E_0}{a} + b, \end{aligned} \quad (S2)$$

where  $a = (\omega_1 + \omega_2)/2W'$  and  $b = (\omega_2 - \omega_1)W'/(\omega_2 + \omega_1)$ . A small factor  $W' = 0.9875$  is introduced to make the algorithm perform better. The rescaled resolvent can be expanded by Chebyshev polynomials

$$\frac{1}{\pm z' - H'} = \sum_n \alpha_n^\pm(z') T_n(H'), \quad (S3)$$

where

$$\alpha_n^\pm(z) = \frac{2 - \delta_{n,0}}{(\pm z)^{n+1} (1 + \sqrt{z^2 - 1})^n \sqrt{1 - \frac{1}{z^2}}}. \quad (S4)$$

The Green's function  $G_{ij,\sigma}^+$  can be written as

$$G_{ij,\sigma}^+(z') = \frac{1}{a} \sum_{n=0}^{N_c-1} g_n^J \alpha_n^+(z') \mu_n^+, \quad (S5)$$

where  $N_c$  is the cutoff of the polynomial order, and  $g_n^J$  is the Jackson damping factor for suppressing Gibbs oscillations [62]. The Chebyshev moments  $\mu_n^+$  are given by

$$\mu_n^+ = \langle \psi_0 | c_{i\sigma} T_n(H') c_{j\sigma}^\dagger | \psi_0 \rangle = \langle \psi_0 | c_{i\sigma} | t_n \rangle. \quad (S6)$$

The Chebyshev vector  $|t_n\rangle$  can be computed iteratively

$$\begin{aligned} |t_0\rangle &= c_{i\sigma}^\dagger | \psi_0 \rangle, \quad |t_1\rangle = H' |t_0\rangle, \\ |t_{n+1}\rangle &= 2H' |t_n\rangle - |t_{n-1}\rangle. \end{aligned} \quad (S7)$$

During calculation, we reduce the bond dimension of MPS using the variational compression method [35, 63]. The ground state is obtained with a bond dimension  $D = 2000$ , and then compressed to  $D_c = 200$  during the Chebyshev iteration. The results remain qualitatively unchanged with larger bond dimensions  $D = 2500$  and  $D_c = 250$ . The number of Chebyshev moments is cutoff as  $N_c = 500$ , which is large enough to clearly show the DOS structure. For  $G_{ij,\sigma}^-(z)$ , it is similar to computing  $\mu_n^- = \langle \psi_0 | c_{j\sigma}^\dagger T_n(H') c_{i\sigma} | \psi_0 \rangle$ . Putting them together, we finally obtain the lattice Green's function

$$G_{ij,\sigma}(z') = \frac{1}{a} \sum_{n=0}^{N_c-1} g_n^J (\alpha_n^+(z') \mu_n^+ - \alpha_n^-(z') \mu_n^-). \quad (S8)$$

### Appendix B: More Results for the one-hole case

In the one-hole scenario, we observe that the four-lobe clover pattern, as seen in the experiment, has its center at the Cu site rather than the Na-doped site. Our analysis suggests that nearby impurities may break the symmetry of the potential fields originally induced by Na doping, resulting in a maximum potential field at a particular site. To further investigate this phenomenon and understand how the LDOS patterns evolve with the potential distribution, we examine more one-hole cases. We start by considering a symmetric configuration, as shown in Fig. S1(a-e). In this setup, the lower-energy state indicated by the red arrow suggests that a single-hole state influenced solely by the potential fields centered on the Na site would manifest itself as a linear superposition of four-lobe clovers on the surrounding Cu sites. This would result in a larger four-lobe clover centered on the Na site. However, as we vary the potential field at the lower right lattice site (see Fig. 1(f-y)), we observe that the larger clover gradually shifts toward the lower right corner and eventually transforms into a configuration similar to the four-lobe clover centered on the Cu site. This evolution is consistent across different higher-energy states, indicating that it is related to changes in the potential fields.

### Appendix C: More Results for the two-hole case

In addition to understanding the one-hole scenario, we are interested in exploring the behavior of two-holes within the lattice. Specifically, our aim is to investigate how local potential fields influence the resulting LDOS patterns. As shown in Fig. S2(a-d), when the local potential fields are uniform, the LDOS exhibits multiple intersecting stripes rather than a three-stripe structure. However, as we introduce an asymmetry between two columns of potentials (Fig. S2(e,i)), the stripe pattern starts to emerge (Fig. S2(g,k)). At the same time, the ladder-shaped pattern becomes more pronounced (Fig. S2(h,l)). These findings suggest that a two-hole state would not manifest itself as a three-stripe pattern if the potential field is completely uniform but would instead appear with an axial bias. This axial bias may arise from impurities or correlation effects among multiple holes, which can alter the effective local potential fields and the resulting LDOS patterns.

### Appendix D: More Results for the four-hole case

We conclude our investigation by exploring the behavior of four holes within the lattice. Our analysis begins with the scenario where there are no impurity potential fields, as depicted in Fig. S3(a-e). In this case, the ground state exhibits a uniform hole distribution without magnetic moment. However, the lower-energy LDOS (Fig. S3(d)) still displays two distinct plaquettes. Upon closer inspection, we find that the hole distribution within these plaquettes does not show a striped pattern. As shown in Fig. S3(f), the LDOS distribution along the red cut line in Fig. S3(d) exhibits four peaks with intervals of  $1.13a_0$ ,  $0.84a_0$ , and  $1.20a_0$  from left to right. The side peaks are taller than the middle ones. When a uniform potential field is introduced (Fig. S3(g-l)), we observe that the stripe pattern becomes evident and the stripe order emerges in the ground state. This indicates that the impurity potential can stabilize the stripe order and the corresponding LDOS pattern. As depicted in Fig. S3(l), the LDOS distribution along the red cut line in Fig. S3(j) still shows four peaks, but now the middle two are the tallest, with peak spacings of  $1.20a_0$ . Finally, we modulate the potential field to be stronger on one side (Fig. S3(m-r)), resulting in only three stripes being evident in Fig. S3(r). The rightmost peak is significantly lower than the others, with distances between neighboring peaks ranging from  $1.2a_0$  to  $1.3a_0$ , consistent with experimental observations. These results further emphasize the significance of impurity potentials and correlation effects between multiple holes.



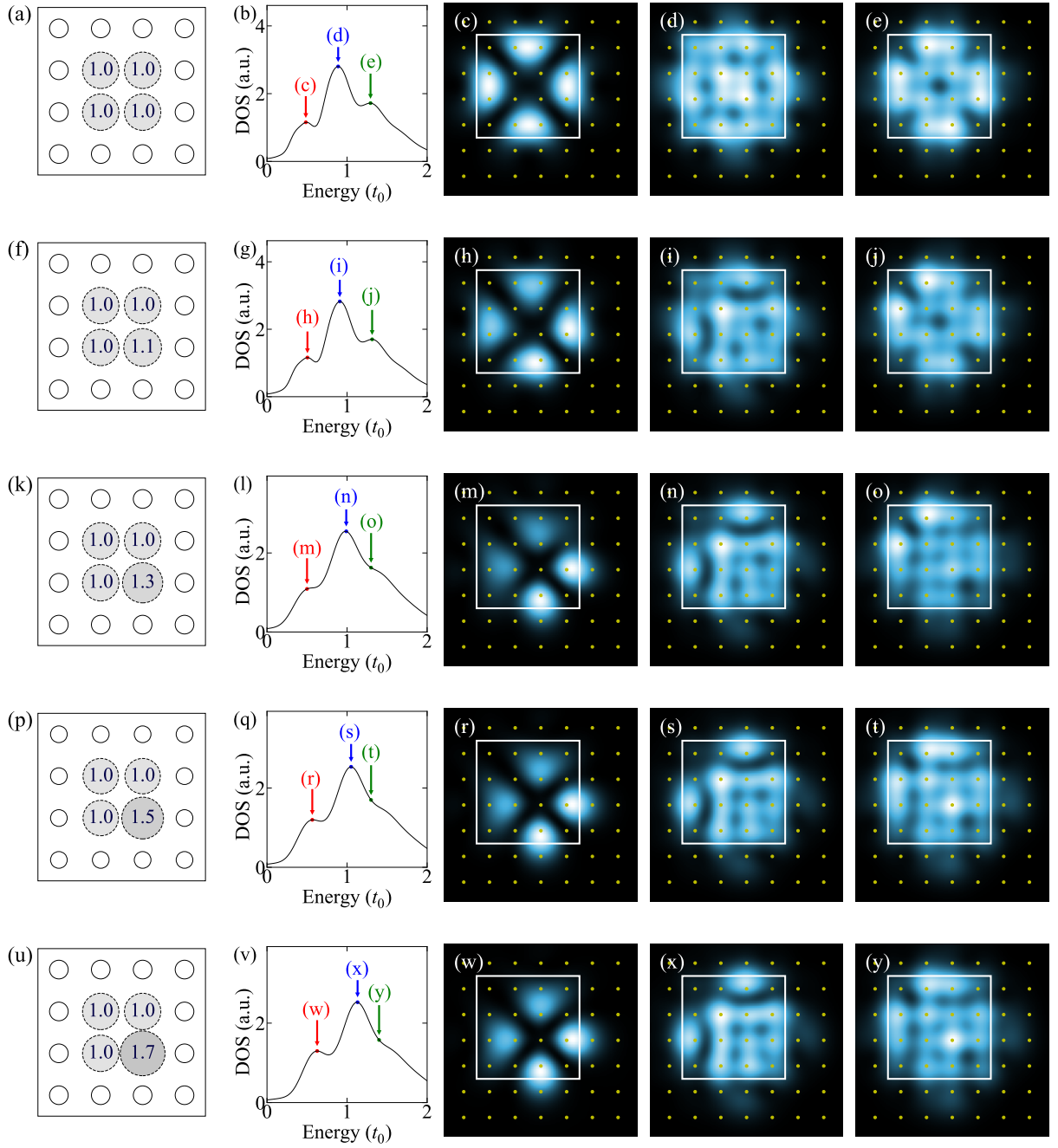


FIG. S1. LDOS patterns for one-hole cases under various impurity potentials. For all cases, the chemical potential is  $\mu = -3.7t_0$ .

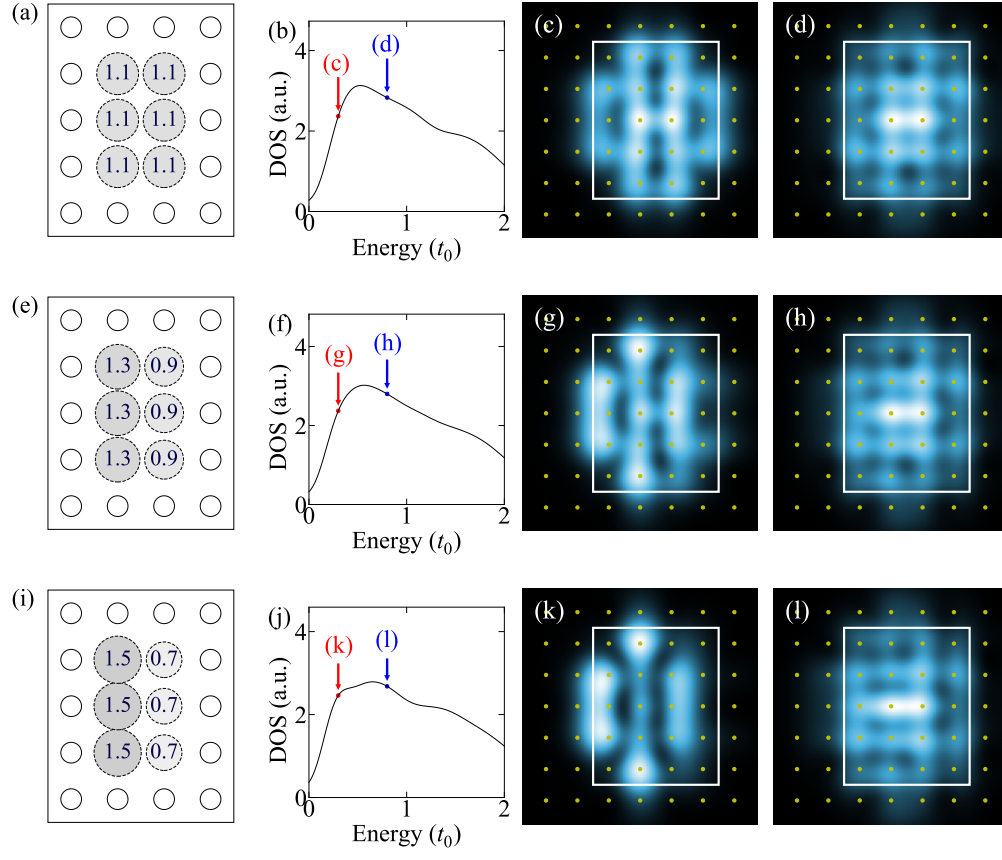


FIG. S2. LDOS patterns for two-hole cases under various impurity potentials. For all cases, the chemical potential is  $\mu = -3.7t_0$ .

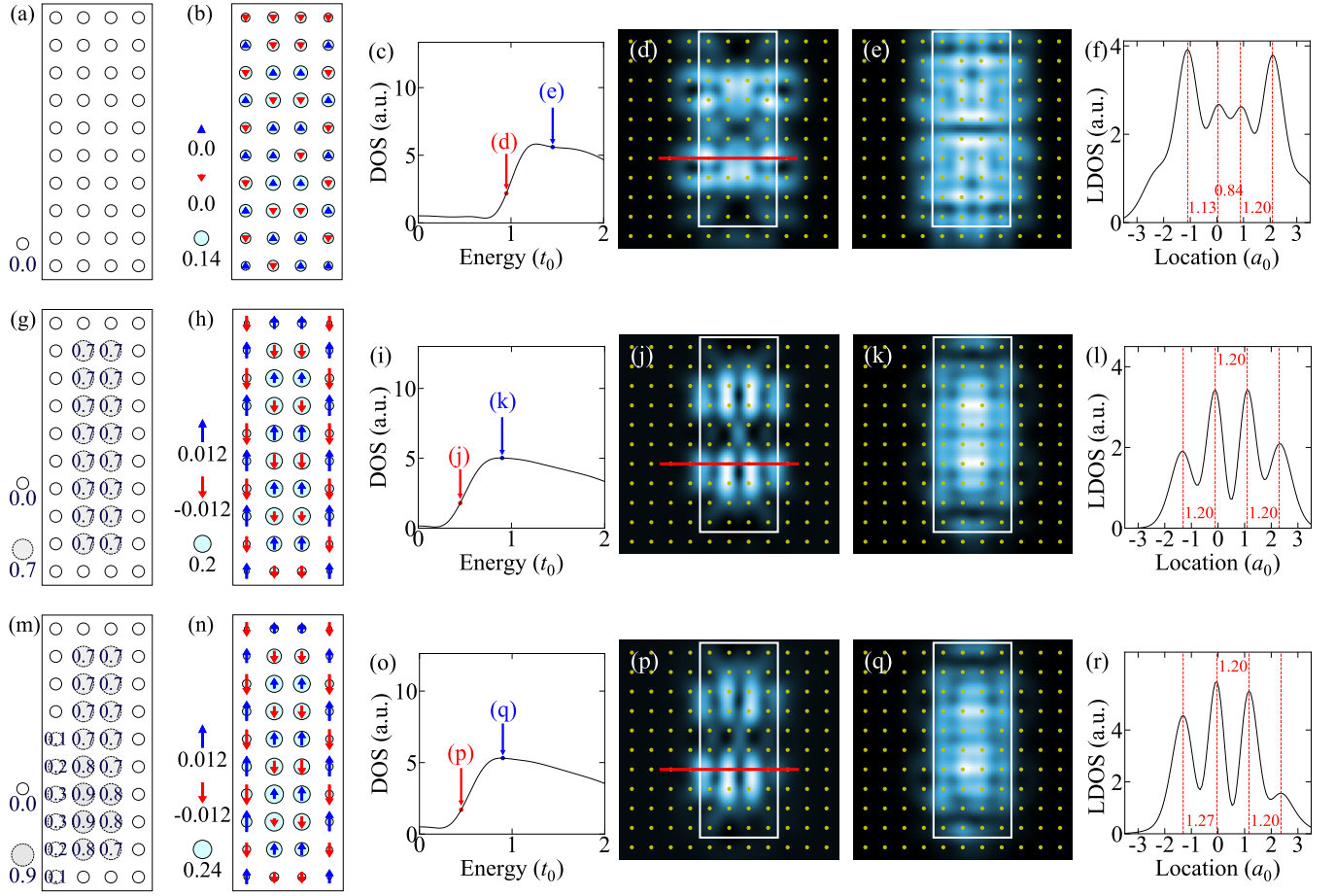


FIG. S3. LDOS patterns for four-hole cases under various impurity potentials. For (a-f), the chemical potential is  $\mu = -4.5t_0$ . For (g-l) and (m-r), the chemical potential is  $\mu = -3.7t_0$ .